RSC Sustainability

ROYAL SOCIETY OF CHEMISTRY

PAPER

View Article Online
View Journal

Cite this: DOI: 10.1039/d6su00116e

Self-assembled carbazole amphiphiles for postharvest monitoring of pest infestation through uric acid detection

Harshal V. Barkale and Nilanjan Dey *

Two carbazole-based fluorescent amphiphilic probes were synthesized and systematically investigated for the selective recognition of uric acid (UA). The probes exhibit a distinctive concentration-dependent dual fluorescence response toward UA, originating from a hierarchical binding mechanism. At low UA concentrations, electrostatic association between protonated piperazine units and urate anions induces fluorescence quenching, while at higher concentrations, cooperative hydrogen bonding and π–π stacking interactions involving carbazole moieties lead to pronounced fluorescence enhancement through excimer-state redistribution. Probe 2 shows a detection limit as low as ~0.6 μM. Detailed spectroscopic, lifetime, and mechanistic studies confirm the formation of static probe-UA complexes and modulation between monomeric, partially overlapped, and fully overlapped excimer emissions. Importantly, the sensing platform remains operational in complex food matrices; fluorescence titrations performed in rice and other cereal extracts display excellent linearity and selectivity toward UA with negligible interference from common cereal constituents. Quantitative estimation of UA in real rice and wheat extracts correlates strongly with conventional enzymatic uricase assays, validating the reliability of this non-enzymatic, multiparametric fluorescence strategy. The method provides a rapid, interference-free, and field-deployable approach for early detection of pest infestation and contamination in stored cereals, supporting sustainable postharvest management.

Received 24th February 2026
Accepted 22nd May 2026

DOI: 10.1039/d6su00116e

rsc.li/rscsus

Sustainability spotlight

This work presents a non-enzymatic fluorescence-based sensing platform for rapid detection of uric acid as a chemical marker of pest infestation in stored cereals. The carbazole amphiphile probes enable sensitive and selective monitoring of grain deterioration in complex food matrices without relying on enzyme-mediated assays, thereby reducing operational complexity, reagent instability, and analytical cost. The sensing strategy supports early identification of storage-related contamination in staple grains such as rice, wheat, and maize, helping minimize postharvest losses, food wastage, and associated economic burdens. By facilitating low-cost, rapid, and interference-free food quality assessment, the study contributes toward sustainable food storage, improved supply-chain management, and enhanced food security in resource-limited settings.

Introduction

Estimated postharvest grain losses are in excess of 10–20% per annum globally, corresponding to approximately 144 million tons of cereal grains and $1 trillion in value overall, while in developing countries potentially experience between 10–30% losses mainly because of inefficient storage practices (inadequate silos, high humidity), out-of-control insect infestations, poor transportation infrastructure (open trucks contaminating grains with moisture/pests), and careless loading/discharging practices contributing to accelerated spoilage by contamination.[1] Stocked grains are most at risk to primary pests in the form of *Sitophilus oryzae* (rice weevil), *Rhyzopertha dominica* (lesser grain borer), and secondary pests, including *Tribolium castaneum* (red flour beetle), which proliferate undetected in bulk storage and deposit nitrogen-rich UA excreta as their principal metabolic waste.[2] This UA can act as a highly sensitive and specific quantitative indicator for observed levels of grain damage due to a linear correlation to insect population density, actual feed times, and ensuing grain degradation levels (primarily free fatty acids, mycotoxins, off-odors), even before visible frass, webbing, or weight loss manifests, enabling early intervention to preserve quality.[3]

Traditionally, UA is quantified using uricase-mediated enzymatic assays, where it is oxidatively decomposed to produce allantoin and hydrogen peroxide, the latter being detected *via* colorimetric methods.[4] Despite their widespread use, these assays suffer from notable limitations, including interference from endogenous biomolecules such as bilirubin

Department of Chemistry, BITS-Pilani Hyderabad Campus, Hyderabad-500078, India. E-mail: nilanjan@hyderabad.bits-pilani.ac.in

and ascorbate, long incubation times (~30 min), and strict requirements for pH and temperature control.[5] Although several small organic molecule-based optical probes have been explored as alternatives, many exhibit poor selectivity and diminished response toward UA in aqueous and complex matrices.[6] Most reported receptors rely primarily on hydrogen-bond-donating motifs such as amide, urea, thiourea, pyrrole, or phenol units, which often lack sufficient discrimination in real biological and food samples.[7] Among various nitrogen-containing spacers, piperazine offers several advantages for supramolecular sensing in aqueous media. The presence of two protonatable nitrogen centers provides moderate aqueous compatibility and enables electrostatic interactions with anionic analytes such as urate under near-neutral conditions. In addition, the conformational flexibility and hydrogen-bonding capability of piperazine facilitate adaptive host–guest interactions and promote the formation of supramolecular assemblies. Importantly, the piperazine spacer also regulates the spatial orientation and intermolecular distance between carbazole chromophores, thereby influencing aggregation behavior, excimer formation, and excited-state fluorescence modulation. These combined characteristics make piperazine an effective structural and recognition unit for designing UA-responsive fluorescence probes.

Considering these aspects, we designed two carbazole-based fluorogenic amphiphiles (1 and 2) for the selective sensing of UA in aqueous media. Carbazole, a nitrogen-fused polyaromatic and planar chromophore, was chosen as the signaling unit owing to its excellent photostability, biocompatibility, and versatile optoelectronic characteristics.[8,9] Owing to its rigid π-conjugated framework, carbazole is widely employed as a donor or π-bridge component in electron donor–π–electron acceptor (D–π–A) architectures and has found extensive applications in dye-sensitized solar cells, light-emitting diodes, photoconductors, and organic field-effect transistors.[10] In the present study, we aim to harness the intrinsic optoelectronic and self-assembly properties of carbazole-based amphiphiles for biomolecular recognition. While optical sensors are attractive due to their structural tunability and operational simplicity, many such systems function primarily as qualitative "yes–no" sensors and often lack reliability in quantitative analysis of complex real samples.[11,12] To address this limitation, the current work focuses on developing a sensing platform that integrates fluorescence intensity modulation, excited-state dynamics, and aggregation-state variation as complementary optical readouts.

Such a multiparametric optical approach enhances analytical confidence by minimizing background interference and false responses.[13–15] Importantly, this strategy provides a foundation for the future development of low-cost, self-monitoring optoelectronic sensing. By enabling rapid, interference-free UA detection in rice/wheat/maize extracts, validated against uricase, the probes offer a novel non-enzymatic tool to monitor pest-derived UA as a proxy for infestation, curbing wastage and enhancing grain supply chain integrity.

Results and discussion

Design and synthesis of probe molecules

We have designed and synthesized two carbazole-based amphiphilic dyes with piperazine as the hydrophilic spacer unit in this work (Fig. 1). Compounds **1** and **2** were synthesized

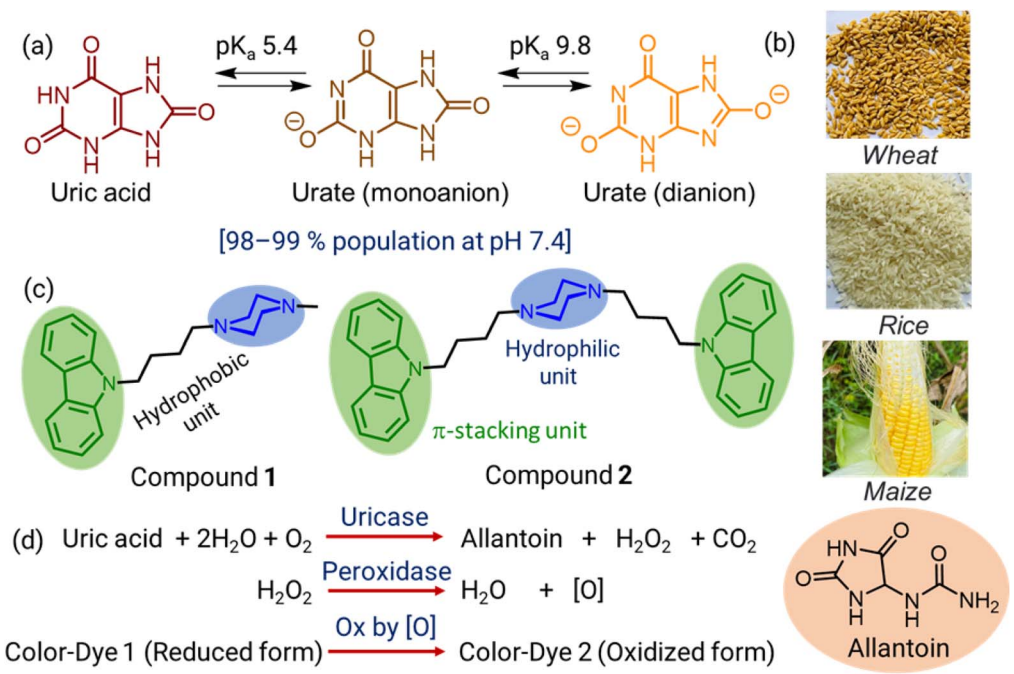

Fig. 1 (a) pH-dependent protonation equilibrium of uric acid. (b) Uric-acid-rich staple foods are mostly available in the Indian subcontinent. (c) Chemical structures of compounds (**1**, **2**) involved in the present study. (d) Clinically-approved enzymatic (uricase) assay available for the determination of uric acid.

following the procedure reported in the literature with slight modifications.[16] Characterisation data for both compounds are attached in the SI (Fig. S1–S6). In the case of compound **1**, the carbazole and piperazine are separated by a C_4-alkyl spacer, while for compound **2**, it acts as a bridging unit between two carbazole units. In neutral pH, piperazine mostly remains in monocationic protonated form (p*K*a: 9.78 and 8.31 for 1,4-dimethyl piperazine).[17] Thus, one can expect the formation of self-assembled structures in the aqueous medium. However, the extent of aggregation will be somewhat inferior compared to 2,7-disubstituted carbazole derivatives with extended conjugated structures. UA undergoes sequential deprotonation with p*K*a1 ≈ 5.4 and p*K*a2 ≈ 9.8, resulting in the predominance of the monoanionic urate species (~98–99%) at pH 7.4. (Fig. 1a) This negatively charged form facilitates electrostatic association with the protonated piperazine units of the probes, forming the basis of the sensing mechanism. In contrast to conventional uricase–peroxidase assays, which rely on enzymatic oxidation of UA to allantoin and subsequent H_2O_2-mediated signal generation, the present system enables direct fluorescence recognition through supramolecular interactions (Fig. 1d).

Photophysical properties of 1 and 2

The UV-visible absorption spectra of **1** and **2** exhibit characteristic π–π* transitions of the carbazole framework at ~270 nm and ~330 nm, along with a weak n–π* band near 370 nm (Fig. 2a). Notably, **2** shows higher overall absorbance intensity and broader spectral features compared to **1**, which can be attributed to the extended π-conjugation and additional stacking interactions introduced by its bis-carbazole architecture.[18] The fluorescence spectra of **1** and **2** ([1] = [2] = 10 μM) in solvents where the probes remain molecularly well-dispersed, such as THF, exhibited characteristic "carbazole-like" emission with well-resolved vibronic features (Fig. S7 and S8). Generally, the fluorescence bands in the 340–360 nm region can be assigned to monomer emission, while the peaks appearing between 360–430 nm are attributed to partially overlapped excimer states. To further investigate the influence of the solvent environment on the excited-state behavior, the fluorescence spectra of **1** and **2** were recorded in solvents of different polarity. Both probes displayed relatively structured vibronic emission in good organic solvents, indicating predominantly monomeric carbazole emission under well-solvated conditions. However, with increasing solvent polarity and aqueous content, gradual spectral broadening and red-shifted emission characteristics were observed, particularly for **2**. The enhanced long-wavelength emission in aqueous medium suggests aggregation-assisted excimer formation arising from hydrophobic association and π–π stacking interactions between carbazole units. These solvent-dependent spectral variations further support the aggregation-regulated fluorescence behavior proposed for the present system.[19] A broad, redshifted emission band centered at about 470 nm was observed explicitly for compound **2**, which suggests an intramolecular π-stacking interaction. The emission due to the full overlap excimer is

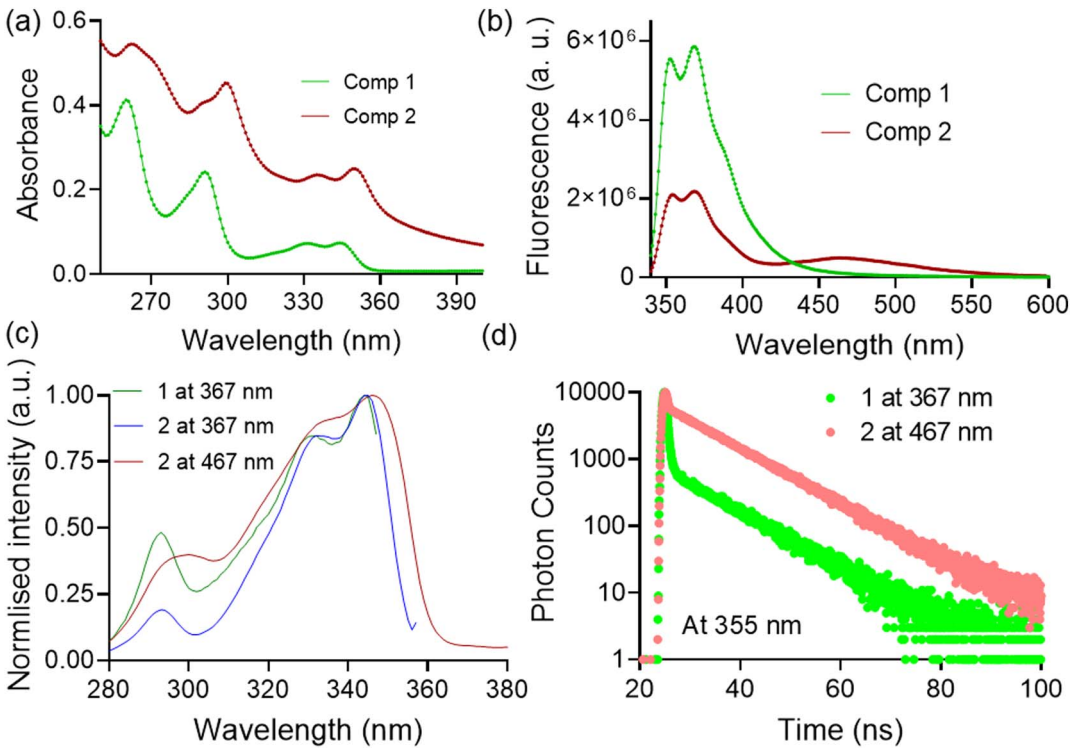

Fig. 2 (a) UV-visible spectra of **1** and **2** (10 μM) in buffered medium (pH 7.0). (b) Fluorescence spectra of **1** and **2** (λ_{ex} = 340 nm, 10 μM) in buffered medium (pH 7.0). (c) Fluorescence excitation spectra of **1** (10 μM) at 370 and 470 nm in buffered medium (pH 7.0). (d) Fluorescence lifetime spectra of **1** and **2** (λ_{ex} = 340 nm, 10 μM) at 370 nm in buffered medium (pH 7.0).

observed between 430–500 nm. Such electronic coupling of the individual chromophores (carbazole) is expected to stabilize the excited states to a greater extent (of lower energy) and results in the observed redshift in emission maxima.[20,21] In principle, forming a new emissive species *via* π-stacking interaction can be a ground-state phenomenon (before photoexcitation) or an excited-state phenomenon (after photoexcitation). To distinguish between these two possibilities, excitation spectra of **2** in water were recorded at each of the two major emission bands, 370 and 470 nm, respectively (Fig. 2c). A similar excitation spectrum observed in these two emission bands suggests that they originated from the same photoexcited species.

Similarly, the excitation spectra recorded at different emission wavelengths of **1** showed identical features, suggesting the presence of a single photoexcited species. Unlike **2**, compound **1** didn't exhibit excimer or aggregate emission even at longer excitation wavelengths. The powder XRD analysis showed the formation of an additional peak at 23.9° for **2**, which indicates a π-stacking distance of 3.7 A° (ref. 22) (Fig. S9). Further, on raising the temperature of the solution, substantial fluorescence quenching was observed at the excimer band for compound **2**. This might be due to the temperature-induced destacking of carbazole units in the aqueous medium (Fig. S10). Similarly, protonation at the piperazine unit (spacer) could change conformation, diminishing the excimer fluorescence. Time-dependent fluorescence studies with both **1** and **2** indicate a decrease in the average lifetime values of the excited state species on going from THF to water medium (Fig. 2d). This might be due to hydrogen-bonding interactions with solvent molecules. On the other hand, the average fluorescence lifetimes at the 370 nm band were found to be larger than the 355 nm band, irrespective of the solvent system. This is quite expected, as emission at the 370 nm band originated from 'partially-overlapped' excimer, while the monomer species is responsible for the fluorescence band at 355 nm.

Spectroscopic investigations with uric acid

Since the piperazine unit is known as the specific supramolecular host for UA, we were interested in investigating the effect of UA on the fluorescence signal of both compounds **1** and **2**. The addition of UA to the aqueous solutions of both **1** and **2** led to bright blue fluorescence (turn-on response), as observed under a long UV lamp. As expected, an increment of FL intensity by ~2.4-fold was observed when ~1 mM of UA was added to the aqueous solution of **1** (Fig. 3b). On the contrary, compound **2**, under similar conditions, witnessed a ~3.8-fold increment in the FL intensity (Fig. 3d). At the same time, the relative ratios of intensities at excimer (I_E) and monomer (I_M) bands (I_E/I_M ~0.22 to 0.13) also changed upon the addition of UA (Fig. 4a and b). However, an interesting observation was made during the titration studies with UA. At a lower concentration of UA (0 to 0.1 mM), we observed concentration-dependent quenching in fluorescence intensity (Fig. 3a and c). However, the further increase in UA concentration (0.1–1.1 mM) resulted in a drastic

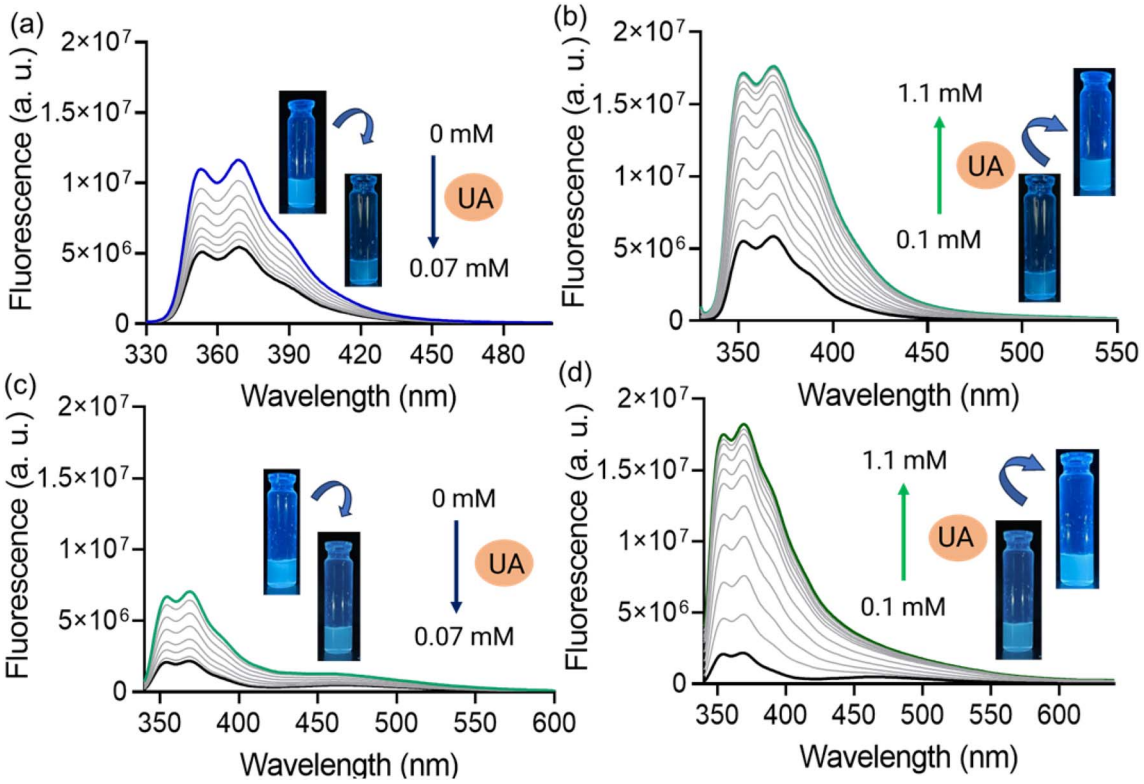

Fig. 3 Fluorescence titrations of (a) **1** and (c) **2** (λ_{ex} = 340 nm, 10 μM) with UA (0–0.07 mM) in buffered medium (pH 7.0). Fluorescence titrations of (b) **1** and (d) **2** (λ_{ex} = 340 nm, 10 μM) with UA (0.1–1.1 mM) in buffered medium (pH 7.0).

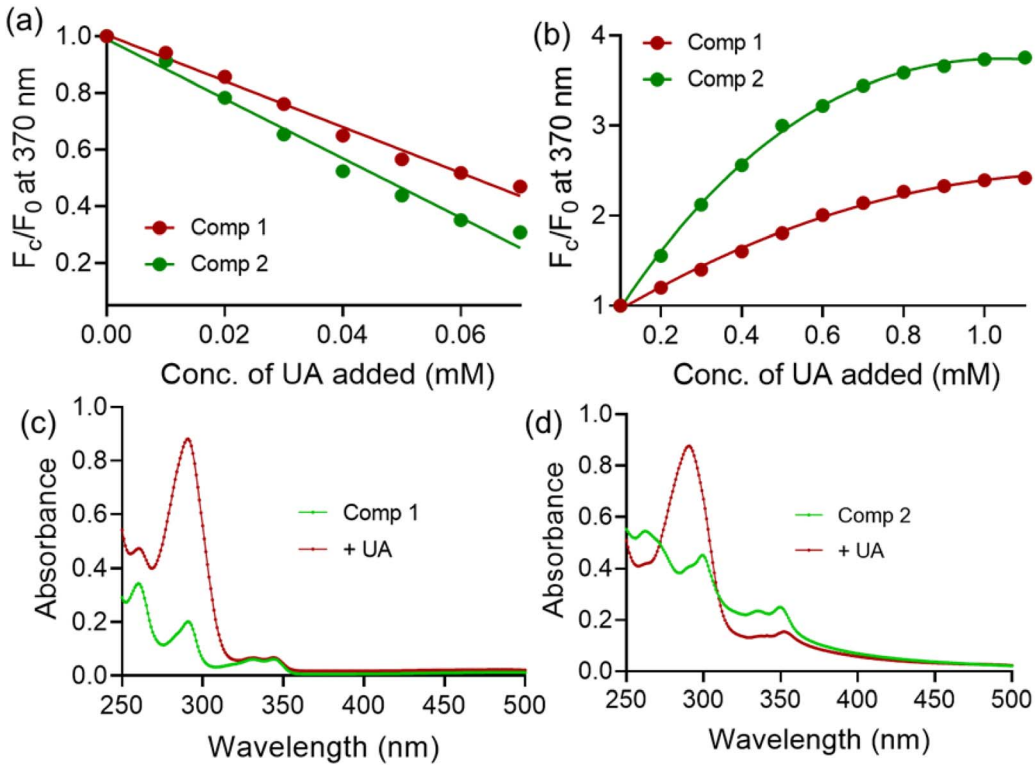

Fig. 4 Change in fluorescence intensity of **1** and **2** (λ_{ex} = 340 nm, 10 μM) at 370 nm upon addition of UA (a) 0–0.07 mM and (b) 0.1–1.1 mM in buffered medium (pH 7.0). UV-visible spectra of (c) **1** and (d) **2** with UA in buffered medium (pH 7.0).

rise in FL intensity. The same was also witnessed during the fluorescence titration of **2** with UA. We believe that such a dose-dependent, abrupt change in FL intensity indicates two different modes of interaction with UA.[23] When we analyze the changes in emission intensities of **2** at different fluorescence bands (354, 392, and 467 nm) upon the addition of UA, we encountered an interesting observation. With a gradual increase in UA concentration, the relative contribution from partially overlapped excimer increases at the expense of fully-overlapped excimer (with respect to the monomer emission). This indicates a change in the conformation (from full- to partially-overlapped excimer) of **2** due to multimodal interaction with UA. The titration studies indicate compound **2** can detect UA as low as ~0.62 μM.

The UV-visible spectral studies suggest that the absorption bands at 332 and 345 nm experience hypsochromic shifts in the presence of UA (Fig. 4c and d). Further, a tailing was observed in the presence of UA, especially on the longer wavelength side, indicative of a charge transfer (CT) process.[24–26] To diagenesis of UA-related diseases, the analysis of biological samples, such as human blood serum or urine, is essential. Since these samples contain a wide range of biomolecules other than UA, we checked the interaction of the compound with other analytes, such as creatinine, cysteine, glucose, dopamine, acetylcholine, ethanolamine, *etc.* Though minor enhancements in FL intensity were observed upon adding a few analytes, such as HSA, glycine, urea, *etc.*, the extents were insignificant compared to that observed with UA (Fig. 7c). The SEM images of both compounds **1** and **2** showed flat tape-like (fragmented) structures, which converted to spherical aggregates in the presence of UA (Fig. 7b).

Mechanistic investigations with uric acid

Spectroscopic and NMR experiments were performed to determine the exact interaction mode with UA. Though the solution-based studies were performed in the aqueous medium, ^{1}H-NMR of compounds (**1**, **2**) with UA was recorded in DMSO-d_6. The aliphatic protons of **2** present near the piperazine unit experienced downfield shifts upon the addition of UA (Fig. S11). This might be due to the hydrogen bonding interaction between the piperazine nitrogen centers and amide –NH groups of UA.[27] On the other hand, the aromatic protons showed distinct upfield shifts upon the addition of UA (Fig. 6). In the case of **1**, the interaction with UA is dominated mainly by hydrogen bonding and electrostatic association involving the piperazine unit, leading predominantly to deshielding effects and consequent downfield shifts. In contrast, for **2**, the presence of two carbazole moieties facilitates aggregation-assisted π–π stacking and conformational reorganization upon UA binding, generating local aromatic shielding effects that result in noticeable upfield shifts. The stronger shielding behavior observed for **2** is also consistent with its excimer emission characteristics and aggregation propensity in aqueous medium. This is presumably due to the formation of the π-stacked sandwiched complex with UA. Similarly, the piperazine protons of **1** showed a similar kind of downfield shift upon the addition of UA. However, the extents of upfield shift at carbazole protons was insignificant. The FT-IR

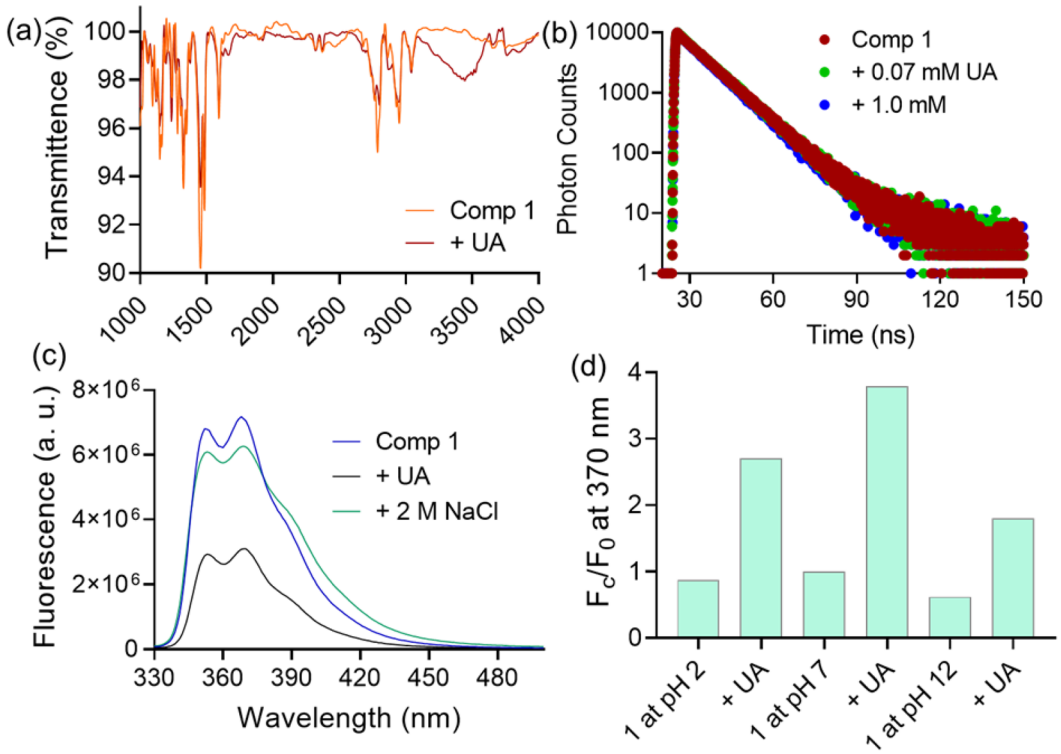

Fig. 5 (a) Partial FT-IR spectra of **1** with UA. (b) Fluorescence lifetime spectra of **1** (λ_{ex} = 340 nm) at 370 nm upon addition of UA in buffered medium (pH 7.0). (c) Fluorescence spectra of **1** (λ_{ex} = 340 nm, 10 μM) with UA in the presence of NaCl (2 M) in buffered medium (pH 7.0). (d) Change in fluorescence intensity of **1** (λ_{ex} = 340 nm, 10 μM) upon addition of UA at different pH conditions (pH 2, 7, and 12) in buffered medium.

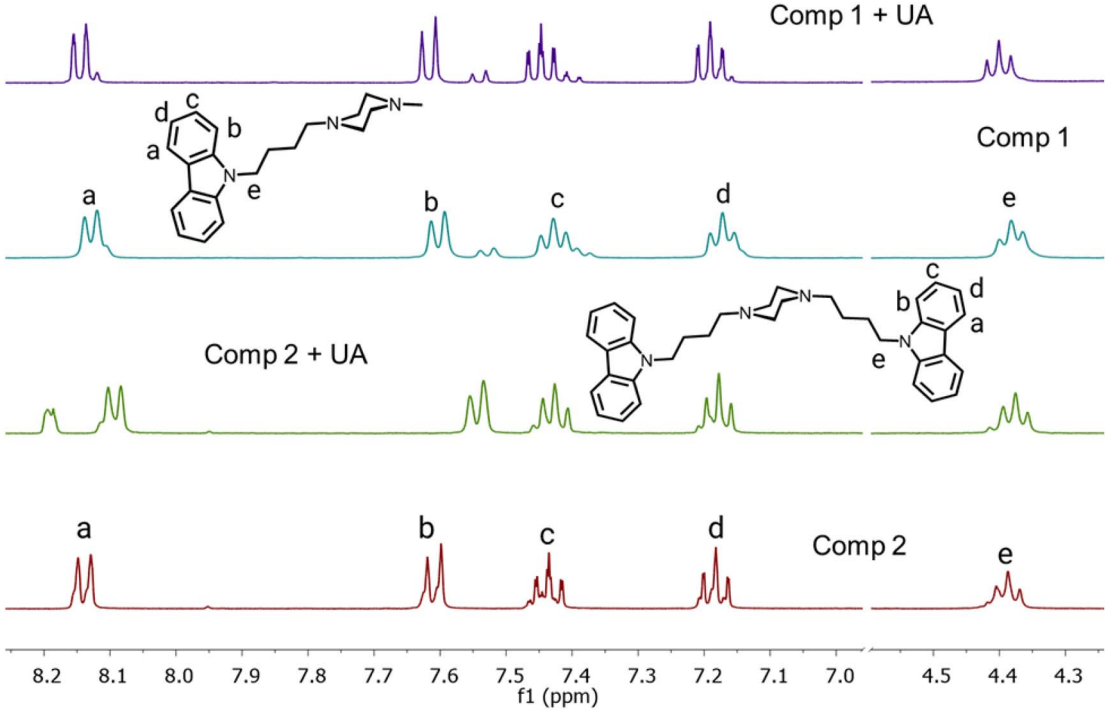

Fig. 6 Partial ^{1}H-NMR spectra of compounds **1** and **2** (5 mM) upon addition of UA (5 mM) in DMSO-d_6 medium.

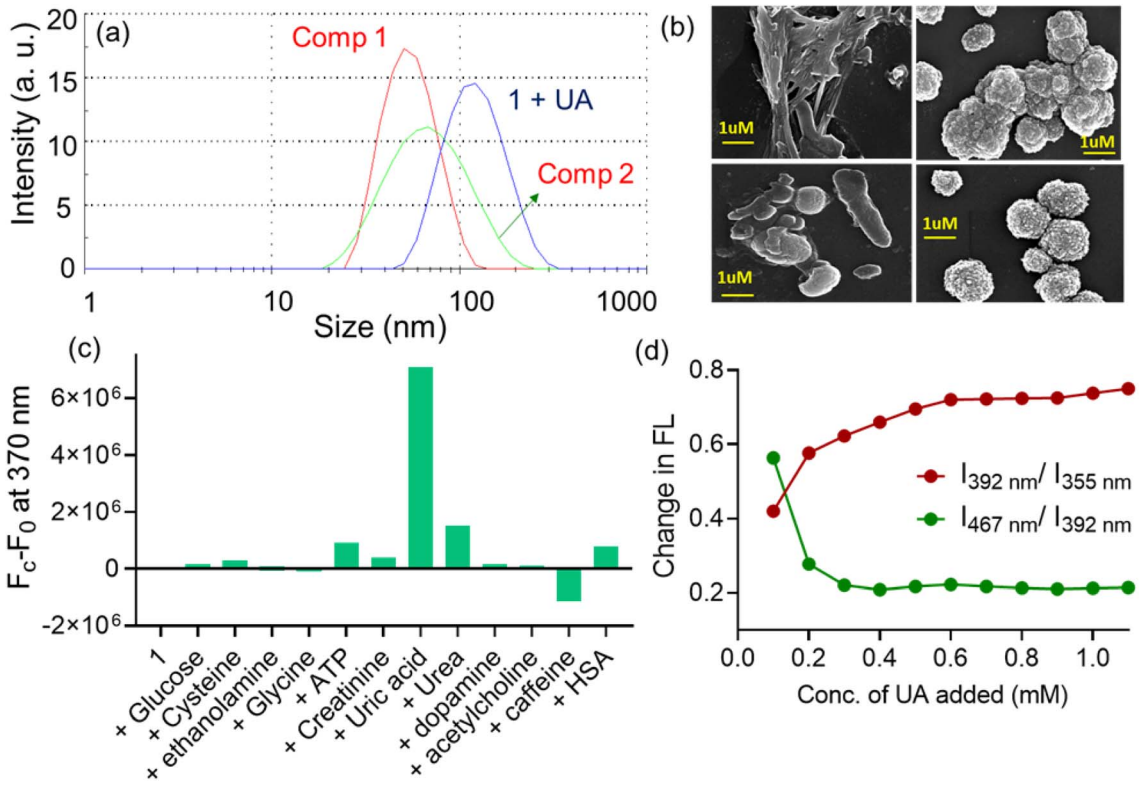

Fig. 7 (a) DLS of compounds **1** and **2** (10 μM) and **1**. UA (10 μM) adduct in buffered medium (pH 7.0). (b) FESEM images of **1** and **2** with and without UA. (c) Changes in fluorescence intensity of **1** (10 μM, $\lambda_{ex} = 340$ nm) at 370 nm upon addition of different biomolecules in buffered medium (pH 7.0). (d) Changes in fluorescence intensity ratios of **1** and **2** upon addition of UA in buffered medium (pH 7.0).

spectra with UA showed the formation of a broad peak in the region of 2470–3305 cm^{-1}, which again confirms the hydrogen-bonding interaction[28,29] (Fig. 5a).

Apart from the hydrogen bonding interaction, we could also expect an electrostatic interaction between compound **1** or **2** and UA. In neutral pH, the compounds will exist in cationic form due to protonation at the piperazine ($pK_a = 9.7$) unit, while UA will be present in monoanionic urate anion ($pK_a = 5.4, 10.3$) form.[30] Since electrostatic interaction/charge pairing sometimes led to fluorescence quenching, we were intrigued to know whether or not the initial fluorescence quenching was due to such a phenomenon. To confirm this, the fluorescence spectra of **1** with UA (80 μM) were recorded at the high salt condition (NaCl = 2 M). No FL quenching was observed in this case, presumably due to the salt-induced screening effect[31] (Fig. 5c). This undoubtedly proved that the formation of the hydrogen-bonded π-stacked complex was initiated by electrostatic interaction (Fig. 9a and b). To confirm this, the responses of **1** with UA were investigated in different buffered conditions (pH 2 and 12) (Fig. 5d). Extents of fluorescence quenching was less in these cases than observed at pH 7. At acidic pH, electrostatic interaction was weak due to the unavailability of the urate anion, while poor interaction at basic pH was due to the scarcity of the protonated form of piperazine. DLS analysis shows a marked increase in hydrodynamic size upon the addition of UA, indicating the formation of aggregated probe-analyte assemblies. The average particle diameter shifts from ~65 nm to ~180 nm for **1** and from ~85 nm to ~210 nm for **2**, confirming aggregation-assisted excimer formation (Fig. 7a). This size evolution corroborates the fluorescence enhancement at higher UA concentrations, where hydrogen bonding and π–π stacking stabilize supramolecular aggregates.

The ratiometric fluorescence response further supports this aggregation-driven mechanism. With increasing UA concentration, the emission intensity ratio I_{392}/I_{355} increases, while I_{467}/I_{392} decreases, indicating a gradual transition from monomeric to excimer-dominated emission states (Fig. 7d). The time-dependent fluorescence studies indicate no change in the average fluorescence lifetime values of **1** and **2** upon addition of UA (70 μM and 1 mM) (Fig. 5b). This indicates the formation of a static complex of probe molecules with UA.

DFT analysis of Comp-1 and uric acid complexation and electronic reorganization

Density functional theory (DFT) calculations were carried out to gain mechanistic insight into the interaction of **1** with UA and to rationalize the experimentally observed fluorescence modulation. For **1** the HOMO is localized on the electron-rich piperazine moiety (Fig. 8b), while the LUMO is located on the electron-deficient carbazole ring (Fig. 8c) with an energy gap of 4.48 eV (HOMO at −0.187 a.u., LUMO at −0.022 a.u.). Within the Comp-1-UA complex, the HOMO orbital increases proximity to the

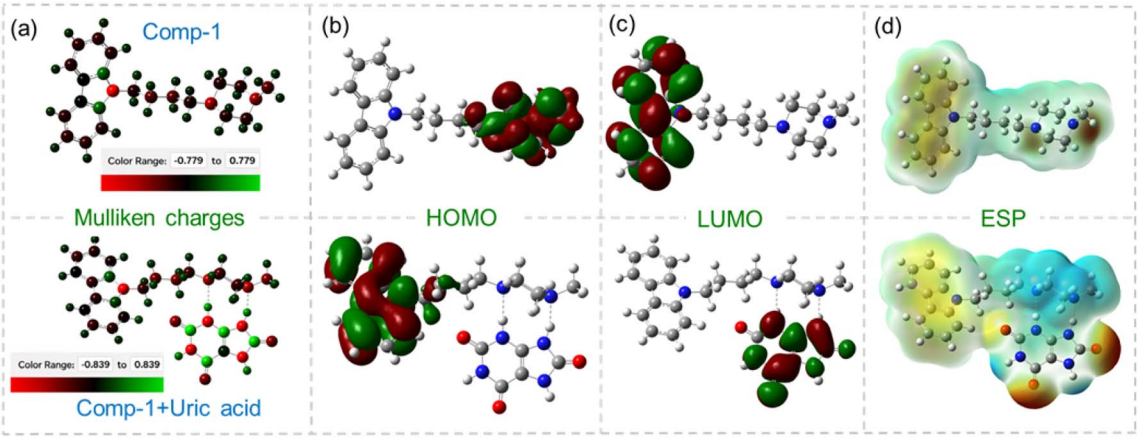

Fig. 8 DFT-calculated (a) Mulliken charge distributions, (b) HOMO, (c) LUMO, and (d) electrostatic potential (ESP) maps of Comp-1 and Comp-1-UA complex. The color scales (−0.779 to +0.779 and −0.839 to +0.839) represent electron-rich (red) and electron-deficient (green) regions, illustrating charge redistribution and orbital delocalization upon interaction.

carbazole donor molecular orbital, while the LUMO orbital expands into the UA acceptor molecular orbital, increasing ICT and decreasing the energy gap to 4.35 eV (HOMO: −0.198 a.u.; LUMO: −0.038 a.u.), which explains fluorescence intensity increase due to UA concentration increase.[32]

Mulliken charge analysis reveals significant charge redistribution, particularly around the piperazine nitrogen centers, crucial for hydrogen bonding. The N1 atom in Comp-1 bears a partial positive charge of +0.463, increasing to +0.510 in the Comp-1-UA adduct, while the N4 atom increases from +0.465 to +0.563 due to greater polarization and more significant electron withdrawal upon the formation of strong hydrogen bonds[33] (Fig. 8a). These charge enhancements (ΔN1 = +0.047; ΔN4 = +0.098) strengthen electrostatic interactions with the UA and rigidify the complex geometry.[34,35] The ESP maps of Comp-1 show positive potential concentrated at the protonated piperazine nitrogens, while contrasting with negative domains on carbazole[36] (Fig. 8d). In the UA adduct, stronger positive regions around the piperazine perfectly complement deep negative potentials on urate O/N atoms, which corroborates the strong electrostatic synergy that drives the H-bonding, complex stabilization, and photophysical response.[37]

The formation of the complex also resulted in a lowering of the dihedral angle in the piperazine ring, specifically near the two nitrogen atoms from 55.37° to 44.37° (Table S1). The total energy reduced from −980.49 a.u. to −1618.36 a.u., while the dipole moment increased from 1.58 D to 8.23 D. These findings are consistent with the formation of a polarized bi-component complex. The optimized Comp-1·UA complex features short N···H–N (1.97 Å, to piperazine N-1) and N···H–N (1.81 Å, to N-4) H-bond distances, indicative of strong interactions. These values fall within the range for robust hydrogen bonds (typically 1.8–2.2 Å), where shorter distances inversely correlate with bond strength due to enhanced orbital overlap and electrostatic attraction. Such directional, strong H-bonds rigidify the complex, complementing the electrostatic preorganization and promoting the observed ICT and excimer stabilization.

Analysis of uric acid in natural water and cereal samples

The present system showed fairly good selectivity towards UA. This is an essential criterion of an ideal sensor, particularly for analyzing real-life samples. Interestingly, the current system showed a concentration-dependent shift from a turn-off (at low UA concentration) to a turn-on (at high UA concentration) response. UA is one of the essential chemical indicators for polluted water, as its presence is mainly attributable to human excreta.[38] As much as 600 mg of UA is excreted per day through the urine of one person.[39] Thus, the concentration of UA in raw wastewater primarily lies in the range of 2–4 mg L^{-1}. Considering these, we have analyzed two different water samples from the laboratory tap and the nearby pond (Fig. 9c). No significant difference was noticed when fluorescence spectra of **1** were recorded in pond and tap water samples. It indicates that levels of UA in these samples are lower than the detectable range reported for the present system. Then, both the samples were treated with 0–20 μM of UA, and the changes in FL intensity were recorded at the 370 nm band. The concentration of UA was purposefully chosen in the micromolar range to mimic the actual real-life situation. A dose-dependent, gradual quenching in FL intensity was noticed in the presence of UA. Further, linear variations in FL intensity were noticed when plotted against the concentration of added UA in both cases. Thus, from these linear regressive equations, one can easily determine the presence of UA in unknown wastewater samples. Furthermore, UA quantification was performed independently using a commercially available uricase assay kit. A comparison with conventional enzymatic assay indicates recovery values from 97.2% to 102.5% for the present system. Additionally, small relative standard deviation values (2.5–4.2%) indicate the high accuracy of the present method for the quantification of UA (Fig. 9d). Therefore, it can be inferred that the current strategy can be pretty reliable for detecting UA in real-life samples. Though a few optical sensors are known in the literature for detecting UA, no effort has been made to analyze wastewater samples.

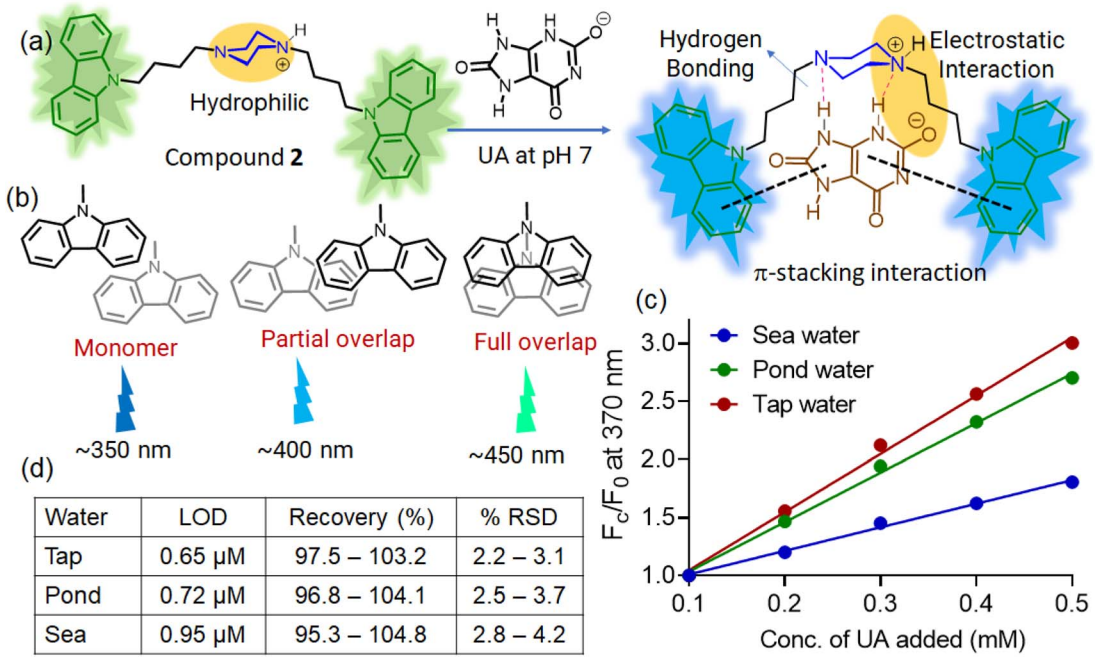

Water	LOD	Recovery (%)	% RSD
Tap	0.65 μM	97.5 – 103.2	2.2 – 3.1
Pond	0.72 μM	96.8 – 104.1	2.5 – 3.7
Sea	0.95 μM	95.3 – 104.8	2.8 – 4.2

Fig. 9 (a) The schematic diagram shows multimodal interactions of compound **2** with UA. (b) Different fluorescence responses for carbazole-based probes, monomer, partially overlapped excimers, and fully overlapped excimers. (c) Change in fluorescence intensity of **2** (λ_{ex} = 340 nm, 10 μM) at 370 nm upon addition of UA spiked water samples (0.1–0.5 mM) in buffered medium (pH 7.0). (d) The table shows analytical parameters for the quantitative analysis of UA in various natural water samples.

Insect infestation in stored grains such as rice, wheat, and maize leads to the accumulation of UA, a nitrogen-rich metabolic byproduct excreted by common storage pests.[40] Monitoring UA levels in these grains provides an effective indirect measure of pest activity and overall grain quality.[41] To replicate real postharvest conditions, the developed fluorescent probes were tested in aqueous extracts of commonly consumed cereal grains spiked with known UA concentrations. These matrices closely mimic the chemical complexity and organic composition of real food systems, allowing reliable evaluation of probe performance under practical conditions.[42] Such analysis bridges laboratory observations with real-world applicability, enabling early and non-enzymatic detection of pest-derived UA contamination in staple grains.

A fluorescence titration experiment was carried out in rice extract to examine whether the probe could function efficiently in a complex biological matrix rich in carbohydrates, proteins, and inorganic salts. (Fig. 1b) Upon gradual addition of UA (0–80 μM) to the rice extract containing the probe, a systematic evolution of the fluorescence spectra was observed, characterized by a concentration-dependent turn-off fluorescence (Fig. 10a). The overall spectral profile and response trend closely resembled those obtained in a buffered aqueous medium, indicating that the intrinsic probe-UA interaction remains intact even in the presence of multiple matrix components. This observation confirms that nonspecific adsorption or competitive binding from rice-derived constituents might not significantly perturb the sensing event. To further establish the generality of the method, similar fluorescence titration studies were extended to extracts of different cereals, including wheat, maize, and other commonly consumed grains (Fig. 10b). In all cases, the probe exhibited fluorescence quenching upon incremental addition of UA, with good linearity over the relevant concentration range. The comparable sensitivity and response slopes across different cereal extracts highlight the matrix-tolerant nature of the amphiphilic carbazole probes and underscore their suitability for routine food-sample analysis. The selectivity of the sensing platform was evaluated by monitoring the fluorescence response in the presence of various potential interferents commonly present in cereals, such as glucose, starch hydrolysates, amino acids, urea, metal ions, and organic acids (Fig. 10c). These analytes induced only negligible changes in fluorescence intensity, whereas the addition of UA produced a pronounced and characteristic response, clearly establishing the high specificity of the probe toward UA under competitive conditions. Finally, the quantitative performance of the developed fluorescence method was benchmarked against the clinically established enzymatic uricase assay[43] (Fig. 10d). UA concentrations determined using the present optical approach in different cereal extracts showed excellent agreement with those obtained from the uricase method, with minimal deviation and high recovery values. This close correlation validates the accuracy and robustness of the non-enzymatic sensing strategy and demonstrates its potential as a rapid, reliable, and interference-free alternative for UA estimation in complex food matrices.

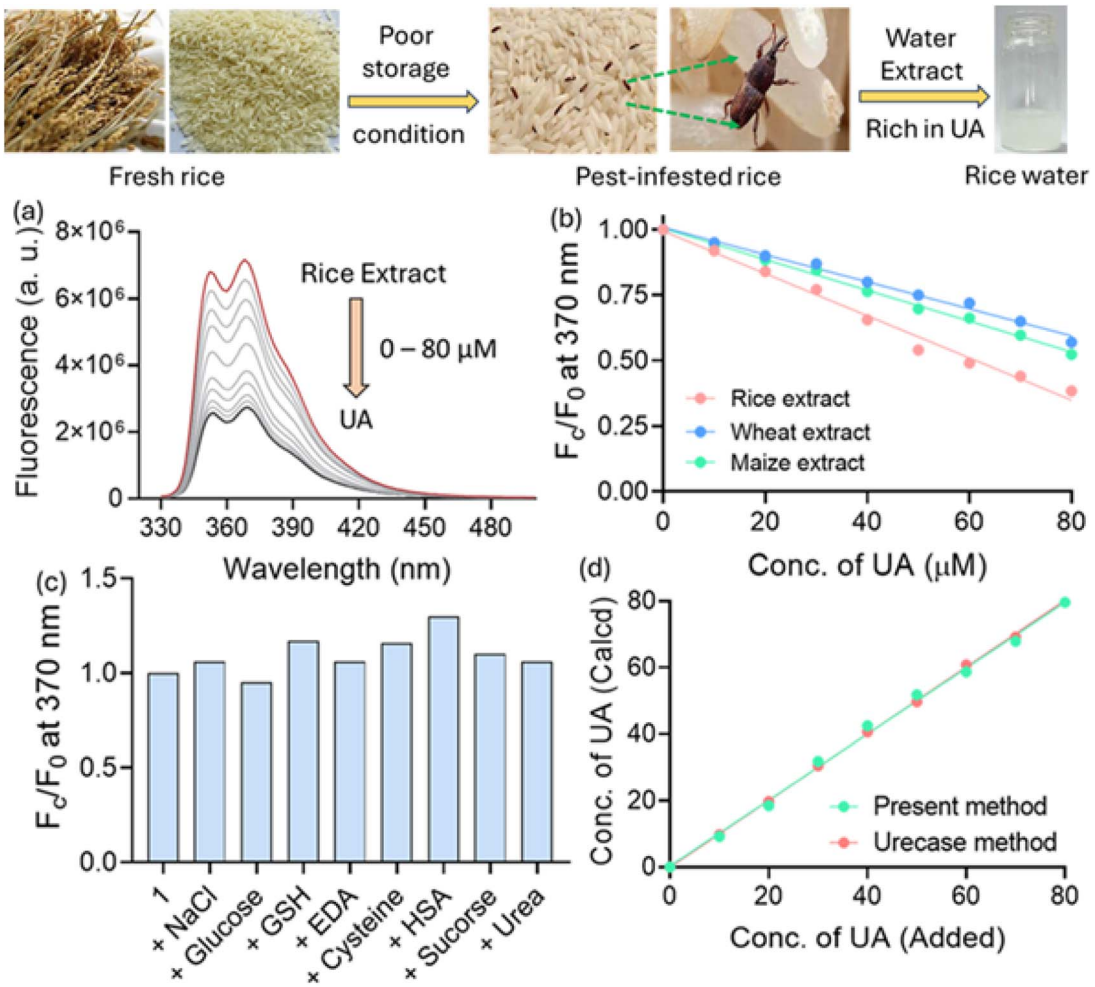

Fig. 10 (a) Fluorescence titration of **1** (10 μM) with rice extract spiked with UA in buffered medium (pH 7.0). (b) Changes in fluorescence intensity of **1** (10 μM, λ_{ex} = 320 nm) at 370 nm upon addition of UA spiked cereal extract (pH 7.0). (c) Interference study showing minimal fluorescence response variation in the presence of common cereal constituents, confirming the high selectivity of the probe toward UA. (d) Quantitative estimation of UA using the present method *vs.* the uricase method.

Conclusion

In summary, two easily synthesizable carbazole-based fluorescent amphiphilic probes (1 and 2) were developed for the selective recognition of UA in aqueous media. Carbazole was chosen as the signaling unit owing to its excellent photostability, biocompatibility, and favorable optoelectronic properties. Both probes exhibited a UA-specific fluorescence response, with probe 2 displaying a low detection limit of ~0.6 μM. Comprehensive spectroscopic and mechanistic investigations revealed a hierarchical, multimodal interaction between the probes and UA, involving initial electrostatic charge pairing between protonated piperazine units and urate anions at low analyte concentrations, followed by cooperative hydrogen bonding and π–π stacking interactions at higher UA levels. This interplay resulted in an unusual concentration-dependent transition from fluorescence quenching to pronounced fluorescence enhancement, accompanied by redistribution among monomeric, partially overlapped, and fully overlapped excimer-emissive states.

Importantly, the sensing platform demonstrated excellent performance in complex matrices relevant to food analysis. Fluorescence titration studies carried out in rice and other cereal extracts showed good linearity, high selectivity, and minimal interference from common cereal constituents, confirming the matrix-tolerant nature of the amphiphilic probes. Given that UA serves as a chemical marker for pest infestation and storage-related deterioration in grains, the present non-enzymatic fluorescence-based approach offers a rapid and reliable strategy for food-quality monitoring. Furthermore, quantitative analysis of UA in real samples showed excellent agreement with the conventional uricase assay, with high recovery values and low relative standard deviations, underscoring the accuracy and robustness of the method. Overall, this work establishes a multiparametric fluorescence sensing platform with broad applicability in biological, environmental, and food-safety analysis.

Author contributions

Harshal V. Barkale: investigation, data curation, validation. Nilanjan Dey: conceptualization, formal analysis, project administration, resources, software, supervision, visualization, writing – original draft, writing – review & editing.

Conflicts of interest

The authors declare no competing financial interest.

Data availability

Data will be made available on request.

Supplementary information (SI) is available. See DOI: https://doi.org/10.1039/d6su00116e.

Acknowledgements

N. D. thanks DST for the SYST grant [grant no. (SP/YO/2021/1632)] and the Ministry of Education (MOE), India, for the STARS grant (STARS2/2023-0300). N. D. and H. B. thank BITS Pilani, Hyderabad campus, for financial and technical support. The authors also thank the central analytical facilities at BITS Pilani, Hyderabad, for instrumental facilities.

References

1 K. Narasimman, A. Pillai, A. Anand, A. Pillai and T. Mathimani, *Sustainable Energy Fuels*, 2025, **9**, 6097–6115.
2 K. D. Ileke and C. O. Adeniran, *Heliyon*, 2025, **11**(2), e41778.
3 A. S. Hashem, H. E. Amin, M. M. Ramadan, A. A. Abdel-Hady, H. S. Awadalla, H. M. Al-Solami, S. E. Sharawi, A. G. Alghamdi, N. A. Alkenani, H. A. Mahran and J. Stored Prod, *Res*, 2025, **112**, 102647.
4 A. Baranwal, S. A. Polash, V. K. Aralappanavar, B. K. Behera, V. Bansal and R. Shukla, *Nanomaterials*, 2024, **14**, 244.
5 S. Aghili, N. Abbariki, H. Daneshgar, M. Edrisi and N. Rabiee, *Anal. Chem.*, 2025, **97**, 23661–23700.
6 J. Li, Y. Xu, Y. Pang, F. Zhao, W. Zhang, C. Li, H. Jin, C. Yuan, S. Wang and Y. Sun, *Chem. Soc. Rev.*, 2026, **55**, 63–113.
7 A. Pal, I. Ahmad and N. Dey, *ACS Appl. Bio Mater.*, 2025, **8**(6), 4699–4706.
8 R. S. Fernandes and N. Dey, *Chem.–Asian J.*, 2025, **20**, e202401354.
9 C. Zeng, S. Liang, J. Lin, W. Liu, Z. Xie, W. Cai, C. Redshaw, X. Feng and B. Z. Tang, *Chem. Sci.*, 2025, **16**, 16719–16728.
10 P. Murugan, T. Hu, X. Hu and Y. Chen, *J. Mater. Chem. A*, 2022, **10**, 5044–5081.
11 A. Xie and W. Wu, *Anal. Methods*, 2025, **17**, 7846–7862.
12 R. S. Fernandes and N. Dey, *J. Mater. Chem. B*, 2024, **12**, 11789–11799.
13 G. Malvicini, J. P. Waclawek, D. Pinto, H. Moser, S. Iadanza, K. Gradkowski, L. O'Faolain and B. Lendl, *Sens. Actuators, B*, 2024, **412**, 135766.
14 M. Sun, K. Huang, Z. Na, Q. Jia, K. Zhou, H. Zeng, J. Zhou, X. Zhang and C. Zeng, *Dyes Pigm.*, 2026, **250**, 113670.
15 S. Liang, J. Li, J. Lin, W. Liu, Z. Na, J. Chen, C. Zeng and X. Feng, *New J. Chem.*, 2025, **49**, 16764–16772.
16 B. Maji, K. Kumar, M. Kaulage, K. Muniyappa and S. Bhattacharya, *J. Med. Chem.*, 2014, **57**, 6973–6988.
17 D. Nemeckova-Herova and P. Pazdera, *Curr. Org. Synth.*, 2015, **12**, 173–179.
18 X. Song, Q. Yu, J. Li, Z. Wu, Y. Xing, Y. Wang, L. Qin, H. Sun, Z. Tie and J. Ma, *Chem. Eng. J.*, 2025, **512**, 162419.
19 G. Reddy, N. Duvva, S. Seetharaman, F. D'Souza and L. Giribabu, *Phys. Chem. Chem. Phys.*, 2018, **20**, 27418–27428.
20 R. M. Adhikari, D. C. Neckers and B. K. Shah, *J. Org. Chem.*, 2009, **74**, 3341–3349.
21 H. V. Barkale and N. Dey, *ACS Appl. Bio Mater.*, 2024, **8**, 189–198.
22 S.-J. Yoon, J. W. Chung, J. Gierschner, K. S. Kim, M.-G. Choi, D. Kim and S. Y. Park, *J. Am. Chem. Soc.*, 2010, **132**, 13675–13683.
23 S. Guo, C. Cheng, Y. Wu, K. Shen, D. Zhang, B. Chen, X. Wang, L. Shen, Q. Zhang and R. Chai, *Adv. Sci.*, 2025, **12**, 2415041.
24 Z. Dong, C. Meng, Z. Li, D. Zeng, Y. Wang, Z. Cheng, X. Cao, Q. Ren, Y. Wang and X. Li, *J. Hazard. Mater.*, 2023, **452**, 131248.
25 H. V. Barkale, A. Narayn, G. Polumati, P. Sahatiya and N. Dey, *ACS Appl. Electron. Mater.*, 2025, **7**(14), 6440–6449.
26 H. V. Barkale, M. Karar, M. Katdare and N. Dey, *J. Ind. Eng. Chem.*, 2025, **159**, 208–217.
27 F.-Z. Wang, H.-Q. Wang, W.-T. Gao and C.-H. Li, *Mater. Chem. Front.*, 2022, **6**, 473–481.
28 M. Akram, H. Lal, S. Shakya and Kabir-ud-Din, *ACS Omega*, 2020, **5**, 3624–3637.
29 H. V. Barkale and N. Dey, *Asian J. Org. Chem.*, 2024, **13**, e202300657.
30 N. G. Lamson, G. Cusimano, K. Suri, A. Zhang and K. A. Whitehead, *Mol. Pharmaceutics*, 2016, **13**, 578–585.
31 A. Adenier and J. Aaron, *Spectrochim. Acta, Part A*, 2002, **58**, 543–551.
32 Z. Xu, F. Liu, T. Zhang, Y. Gu, N. Lu, H. Xu, X. Yan, Y. Song, Y. Xing and D. Yu, *Anal. Chem.*, 2020, **92**, 15297–15305.
33 S. Scheiner, *Phys. Chem. Chem. Phys.*, 2025, **27**(23), 12416–12426.
34 A. Acharya, M. Khanal, R. Maharjan, K. Khanal, K. Gyawali, M. B. Kshetri, R. Adhikari, D. D. Mulmi, T. R. Lamichhane and H. P. Lamichhane, *ChemistrySelect*, 2026, **11**, e04392.
35 S. Pise and N. Dey, *Dalton Trans.*, 2025, **54**, 2896–2907.
36 M. Gayathri, S. Patra, D. Sriram and N. Dey, *J. Mol. Liq.*, 2025, 129000.
37 A. Pal, H. V. Barkale and N. Dey, *Chem.–Asian J.*, 2025, **20**, e202401676.
38 X. Wu, S. Nawaz, Y. Li and H. Zhang, *Environ. Sci. Pollut. Res.*, 2024, **31**, 24745–24767.
39 X. Li, B. Huang, Y. Liu, M. Wang and J.-Q. Cui, *J. Diabetes Its Complications*, 2025, **39**, 108929.
40 J. Xu, Y. Cui, J. Wang, Z. Liu, C. Zhao, Z. Liu, N. Niu, L. Chen, X. Zhao and Y. Fu, *Nanoscale*, 2025, **17**(27), 16153–16192.
41 A. R. Hudu, F. Addy, G. K. Mahunu, A. H. Abubakari and N. Opoku, *Food Sci. Nutr.*, 2024, **12**, 4489–4512.
42 Ranbir, M. Kumar, G. Singh, J. Singh, N. Kaur and N. Singh, *ACS Omega*, 2022, **7**, 47518–47535.
43 S. Tariq, U. Saeed, S. Riaz, A. Saqib, S. Khurshid and M. H. Nawaz, *Mater. Today Commun.*, 2024, **39**, 108902.